ACS OMEGA

Open Access

http://pubs.acs.org/journal/acsodf

Article

Single-Extracellular-Vesicle Detection with a Plasmonic Chip and Enhanced Fluorescence Microscopy

Kazuma Fukutomi, Eri Fujimoto, Masaya Shimokawatoko, Eri Takano, Hirobumi Sunayama, Toshifumi Takeuchi, and Keiko Tawa*

Cite This: *ACS Omega* 2024, 9, 44396−44406

Read Online

ACCESS | Metrics & More | Article Recommendations | Supporting Information

ABSTRACT: Endocytosis-derived extracellular vesicles (EVs), which can be as small as 100 nm, are useful for disease prediction. However, very small EVs are below the optical diffraction limit and are difficult to visualize with conventional fluorescence microscopy. In this study, single EVs captured on a plasmonic chip, where fluorescently labeled antibodies were bound over the EV surface, were detected as bright spots using plasmon-field enhanced fluorescence without any pretreatment of isolating labeled EVs, followed by analyzing the full width at half-maximum and the fluorescence peak value for each enhanced fluorescence bright spot. Bright spots smaller than the threshold determined by the observation of the fluorescent nanospheres were attributed to single EVs. The number of single EVs was quantitatively evaluated against the concentration of EV solution injected in the 1.4 pM−95 fM range. Furthermore, single EVs were detected by labeling two different membrane proteins. A molecularly imprinted polymer was applied to a capture interface on a plasmonic chip, and it is found that nonspecific adsorption of aggregates was suppressed. To accurately distinguish single EVs from aggregates of labeled antibodies, the fluorescence microscopy with transmitted light was superior to the epifluorescence method. Finally, single EVs were successfully detected with multiple targets at multiple wavelengths by using different fluorescently labeled antibodies.

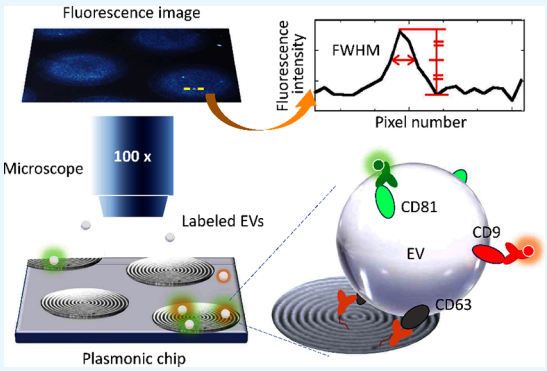

INTRODUCTION

Extracellular vesicles (EVs) are secreted from various cell types, including tumor cells, neurons, B lymphocytes, T lymphocytes, and intestinal epithelial EV cells. EVs exist in various body fluids, including blood, urine, saliva, breast milk, amniotic fluid, ascites fluid, cerebrospinal fluid, bile, and seminal fluid.[1−4] EVs are composed of proteins related to membrane transport, fusion (RabGTPase, annexin, and flotillin), multivesicular body formation (TSG101, Alix), heat shock (Hsc70, Hsc90), cell adhesion (integrin), and transmembrane proteins, such as the tetraspanin family (CD9, CD63, CD81, CD82).[5] Furthermore, EVs also contain raft lipids such as cholesterol, sphingolipids, and ceramides.[6] Currently, the EV formation, biological pathways,[7,8] and biological functions of EVs[9,10] have been clarified but not completely understood. EVs contribute to various physiological and pathological processes, including tumor progression, stimulation of the immune system, coagulation, and inflammation.[1,11] Interestingly, EVs may act as messengers to deliver effectors and signaling macromolecules into inherently specialized intercellular spaces.[12−15] Therefore, detecting and analyzing EVs transferring genetic information may be useful for the diagnosis and prediction of diseases.[16,17] In particular, membrane protein levels in EVs may be linked to cancer dynamics; thus, evaluation of membrane proteins in EVs may provide new modes of cancer diagnosis and prognosis. However, exosomal proteins are difficult to analyze due to their small size and complex composition.[18,19]

EVs are generally detected by Western blotting[20] and enzyme-linked immunosorbent assays after collecting numerous EVs.[21] However, these EV detection methods require many operation steps and large sample volume in mL, and preisolation methods including column chromatography and ultracentrifugation are time-consuming and require special instrumentation. They are a barrier to apply these EV detection techniques to rapid clinical diagnoses.

Single EV detection is not only useful to rapid diagnosis and detailed prediction of diseases but also breakthrough to in situ identify specific cells secreting respective EVs during surgery. Therefore, the development of a simple and compact device for single EV detection and the establishment of a simple and

Received: June 18, 2024
Revised: August 14, 2024
Accepted: October 10, 2024
Published: October 23, 2024

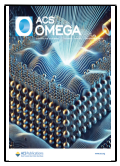

https://doi.org/10.1021/acsomega.4c05678
ACS Omega 2024, 9, 44396−44406

accurate analytical system are urgently required. As one of the most useful tools, flow cytometry analysis (FCM) is widely used in basic research and clinical medicine for the rapid analysis of membrane proteins in single EVs. However, the detection accuracy is insufficient[22] due to the detection limit of >300 nm. According to Liu et al.,[22] EV particle size can be increased to a detectable size in FCM by forming hydrophobic micelles. Rapid and highly sensitive detection of EVs is possible after micelle formation, leading to high-throughput analysis. As another powerful tool, the label-free EV detection method by surface plasmon resonance was proposed.[23−25] Im et al.[23] used periodic nanohole arrays and transmitted surface plasmon resonance. Each array is functionalized with an antibody to enable profiling of membrane proteins at the EV surface and in the EV lysate. This method is more sensitive than conventional analysis methods for the collection of multiple EVs. Furthermore, a single-EV detection technique has been developed.[26,27] Min et al.[26] reported single-EV detection with nanohole array by enhanced fluorescence microscopy. The bright spots corresponding to single EVs were counted by 20-fold enhanced fluorescence, and the relationship between tumor proteins and normal proteins was studied in plasma samples.

In this study, we apply plasmon-enhanced fluorescence to single-EV detection without isolating labeled EVs from free fluorescent antibodies (molecules), which were not bound to EVs by column chromatography and ultracentrifugation. Enhanced fluorescence images can be obtained using plasmonic chips, which are a wavelength-size periodic structure coated with a thin metal film, and they were obtained from epithelial cell adhesion molecules in breast cancer cells[28] and cultured neurons;[29] the enhanced images obtained with epifluorescence and transmitted-light fluorescence microscopy were 10-fold brighter than the images obtained using glass slides and flat metal substrates. For the epifluorescence images of 20 nm-ϕfluorosphere adsorbed on a concentric circle (bull's eye)-patterned plasmonic chip, which has the same structure to that used in this study, 29−36-fold[30] and 6−8-fold enhanced fluorescence images were observed with Cy5 filter units and 10× and 100× objectives, respectively, compared with those on the glass slide. On the other hand, for the fluorescence images of nanofluorospheres under transmitted-light illumination, 20-fold enhanced fluorescence was observed with the Cy5 filter unit and the 100× objective at the bull's eye-patterned plasmonic chip compared with that on the flat silver film without pattern (Figure S1).[31] These enhanced mechanisms are based on the enhanced excitation field and enhanced emission recoupled with a plasmon due to the grating coupled-surface plasmon resonance (GC-SPR).[32,33] The detection and analysis of single EVs were difficult for small fluorescence intensity without a plasmonic pattern. The free electron waves on a metal surface can be coupled with waves of incident light on the grating, and an enhanced electric field is formed under the resonance condition, as described in eqs 1−4.

$$k_{spp} = k_{phx} \pm mk_g \quad (1)$$

$$k_{spp} = (2\pi/\lambda)\sqrt{\varepsilon_1\varepsilon_2/(\varepsilon_1 + \varepsilon_2)} \quad (2)$$

$$k_{phx} = (2\pi/\lambda)\sin\theta i \quad (3)$$

$$k_g = 2\pi/\Lambda \quad (4)$$

where k_{spp} is the wavenumber vector of the surface plasmon polariton, k_{phx} is the wavenumber vector of the x component of the incident light, $k_g$is the wavenumber vector of grating, ε_1 is the complex dielectric constant of a metal, ε_2 is the dielectric constant of a dielectric medium, and Λ is the grating pitch. The enhanced fluorescence results from the excitation field enhancement and the surface plasmon recoupled emission.[33,34]

The goal of this study is to detect single EVs without separating EVs from free fluorescently labeled molecules before adding to a sensor chip by ultracentrifuge and column chromatography and to evaluate the number of EVs simply and quantitatively using a plasmonic chip and fluorescence microscopy. We have used periodic structures, such as a one-dimensional line-and-space structure and a two-dimensional hole array structure, for the fluorescence imaging of cells and immunosensors. However, for this study, we adopted an array of bull's eye patterns composed of concentric circles (Figure 1)

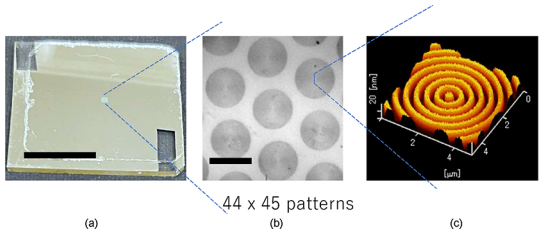

Figure 1. Plasmonic chip: (a) photograph (bar corresponds to 10 mm), (b) bright-field microscopic image (bar corresponds to 20 μm), and (c) AFM image at a center of a plasmonic pattern.

to utilize incident light with an omnidirectional component in plasmon resonance with the microscope under Köhler illumination. Therefore, the fluorescent images of nanosized EVs are bright enough to appear as luminescent spots using plasmon-enhanced fluorescence.[31] Furthermore, a simple sandwich immunoassay was used to detect single EVs (Figure 2) without pre-separating EVs from the free fluorescently

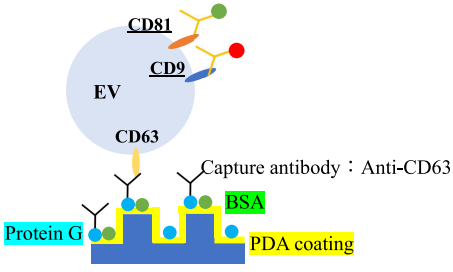

Figure 2. Sandwich assay of single-EV detection on the polydopamine (PDA)-coated surface of a plasmonic chip.

labeled antibody before injection. This process without preisolation will be important to apply this technique to the rapid diagnosis in body fluids. The respective labeled antibodies that did not bind to EVs but adsorbed to the capture interface on the silver plasmonic chip were not observed as bright spots, because of quenching fluorescence by a capture interface composed of polydopamine film and a weak signal of a single labeled antibody (Supporting Information S2). However, around 100 nm-ϕ single EVs bound with some labeled antibodies and aggregates of labeled antibodies appeared as bright spots by enhanced fluorescence on the bull's eye pattern of a silver plasmonic chip with both epi- and

https://doi.org/10.1021/acsomega.4c05678
ACS Omega 2024, 9, 44396−44406

transmitted-light fluorescence microscopes. To distinguish a single EV less than the optical diffraction limit from large grains including aggregates of labeled antibodies, the full width at half-maximum (FWHM) of bright spots was analyzed (Figure S4). Furthermore, the detection accuracy of single EVs was improved by two ways, i.e., modifying the capture surface and the optical system of fluorescence microscopy. To improve the capture interface, the molecularly imprinted polymer (MIP)-based capture interface for EVs reported by Takeuchi's group was applied on the gold plasmonic chip (Figure 3).[35]

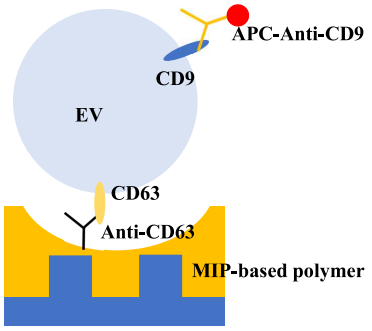

Figure 3. Sandwich assay of single-EV detection on the MIP-based capture interface on a plasmonic chip.

Next, the optics system was changed from epifluorescence to fluorescence excited by transmitted light (Figure 4) to increase

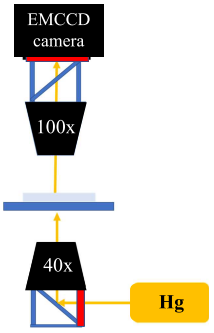

Figure 4. Schematic of an upright-inverted fluorescence microscope with an EM-CCD camera.

the contribution weight of the plasmon-field enhanced fluorescence in the total fluorescence, including plasmon-unrelated fluorescence. EV detection was investigated with the enhanced fluorescence on the silver plasmonic chip under a conventional optical microscope.

On the other hand, single EVs were detected by targeting two different membrane proteins. Thus, single-EV binding to two different fluorescently labeled antibodies was observed as bright spots with two kinds of fluorescent filters under the microscope. The observation of identical bright spots using two different fluorescent filters demonstrates that the measurement and analysis methods for single-EV detection is valid. Multitarget analysis of a single EV is essential for the application to clinical diagnoses.

RESULTS AND DISCUSSION

FWHM for bright spots was analyzed in fluorescent images of nanoparticles as small as EVs below the diffraction limit under each optical condition. The mean FWHM was used as the threshold for distinguishing a single EV in subsequent experiments, as summarized in Table 1.

Table 1. Diffraction Limit Obtained by Analyzing the Full Width at Half-Maximum (FWHM) of the Bright Spots

	epifluorescence		transmitted light	
	threshold/nm	standard deviation/nm	threshold/nm	standard deviation/nm
Cy5	570	60	523	76
GFP	545	47	562	74

Single EVs Observed by Atomic Force Microscopy (AFM). EVs dispersed on the plasmonic chip were observed as bright spots with epifluorescence microscopy. In the fluorescence images, the bright spots with FWHM values below the threshold were considered to be single EVs. After observation of single EVs captured with the chip with a fluorescence microscope, AFM images were taken for the same chip (Figure 5). The diameter of these single particles was 170

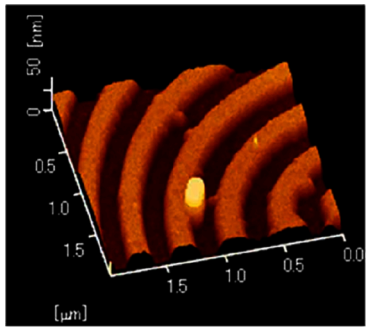

Figure 5. AFM image of a single EV on a plasmonic chip.

± 14 nm in the AFM image, which is an appropriate diameter for EVs. Thus, the bright spots with FWHM values below the threshold in the fluorescence images were assigned to single EVs.

Single-EV Detection by Epifluorescence Imaging with Allophycocyanin (APC)−Anti-CD9 on a Polydopamine (PDA)-Coated Silver Plasmonic Chip. Single EVs were detected by epifluorescence microscopy using a sandwich assay (anti-CD63 and APC-anti-CD9 antibodies for capture and detection, respectively), as shown in Figure 6A. Fluorescence peak intensity and FWHM values were analyzed for each bright spot selected in a bull's eye pattern in the fluorescent images. The fluorescence intensity was plotted against the FWHM. Bright spots with FWHM values below 570 nm were assigned as single EVs (Figure 6A−C). As shown in Figure S5 of the SI, EVs larger than 500 nm contained 1% in the total EVs used in this study. Therefore, the number of EVs was 1% underestimated by this analysis because the bright spots with FWHM larger than threshold were eliminated from single EVs. The mean quantities of single EVs in the reference solution (0 M) and 95 fM and 280 fM EV solutions were calculated from three sheets of fluorescence images. The relationship between the number of single EVs (the number of bright spots) and the EV solution concentration (Figure 6D) was a positive correlation. Although the fluorescently labeled antibody (APC-anti-CD9) concentrations were the same for all EV solutions, the number of single EVs captured by the plasmonic chip and evaluated by this method depended on the EV

https://doi.org/10.1021/acsomega.4c05678
ACS Omega 2024, 9, 44396−44406

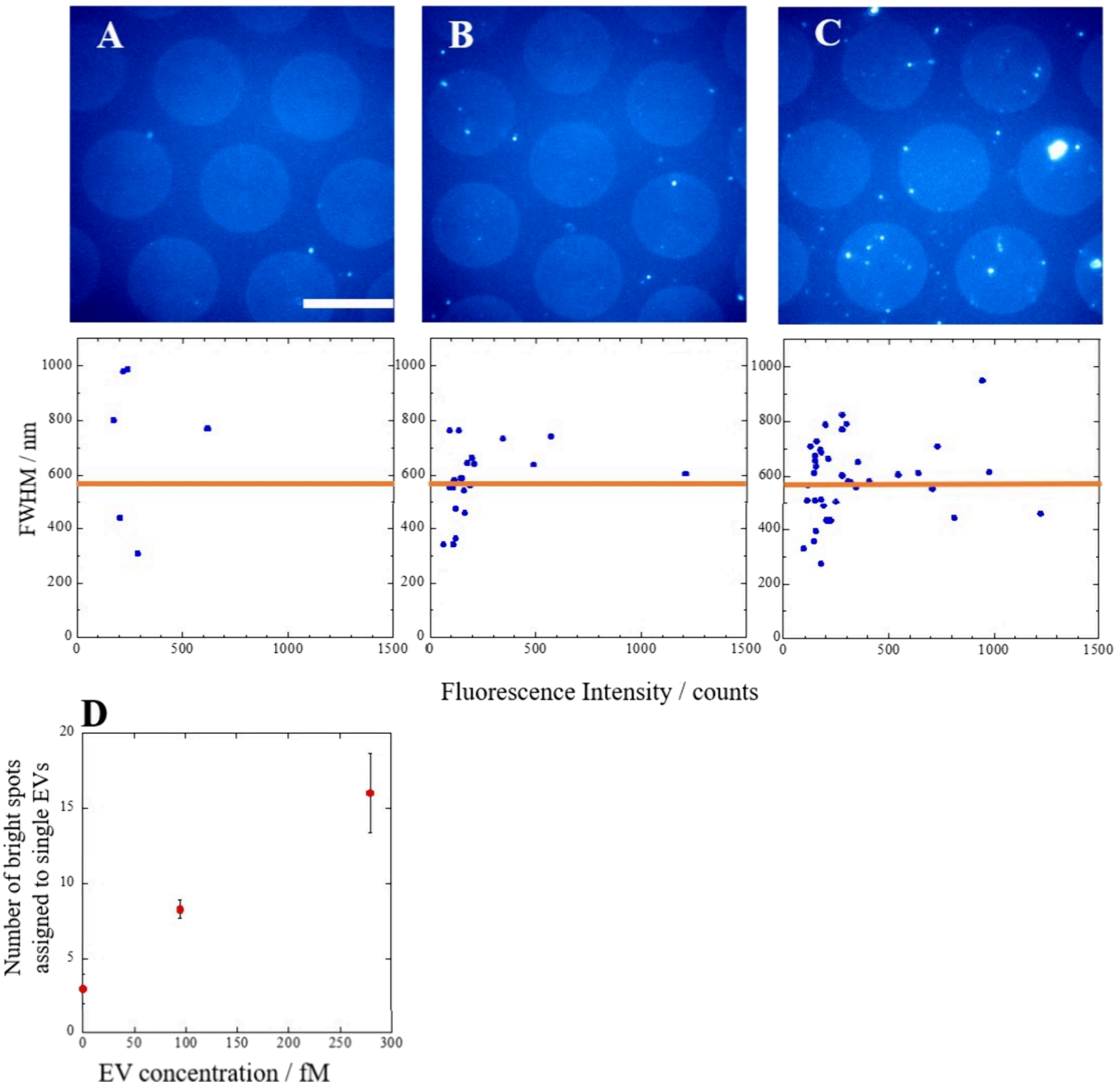

Figure 6. (Upper) Fluorescence images of single EVs detected with APC-CD9 antibody on a plasmonic chip using the epifluorescence system and (middle) the FWHM values plotted against the fluorescence intensities for bright spots detected in (A) 0, (B) 95, and (C) 280 fM EV solutions. Bar corresponds to 20 μm. The orange lines are the threshold for the experimental condition. (D) After analysis of these images, the number of single EVs was plotted against the EV concentrations.

concentration. The detection of single EVs was reproducible. In this measurement, the mixture of fluorescence-labeled detection antibody and EVs was added directly to the capture interface. After rinsing with PBS solution, background light intensity increased due to the excess of free fluorescence-labeled antibodies, but bright spots were not detected. Even excessive fluorescence-labeled antibodies adsorbed at the interface as a single molecule did not appear as bright spots. Large bright spots above the threshold were considered to be due to nonspecific adsorption of detection antibodies or EV aggregates. Therefore, the bright spots observed in the reference solution corresponded to aggregates of the detection antibody. Single EVs were captured and quantitatively evaluated using the sandwich assay on plasmonic chips without any preisolation processes. Based on the calculation that the EV number included in 15 μL (surface area of 1 cm^2 and layer thickness of 150 μm) of solution prepared at 280 fM is 2.5 × 10^6, around 100 EVs are found to exist in a volume on the seven bull's eye patterns (area of 3.6 × 10^{-5} cm^2) inside the microscopic observation area. The mean number of bright points experimentally obtained was 16, and it corresponds to a capture rate of 15−20%. This indicates the validity of the experimental system in this assay.

In the reference solution, around three bright points assigned to single EVs were detected, despite the absence of EVs in the solution. They were considered to be nonspecific

https://doi.org/10.1021/acsomega.4c05678
ACS Omega 2024, 9, 44396−44406

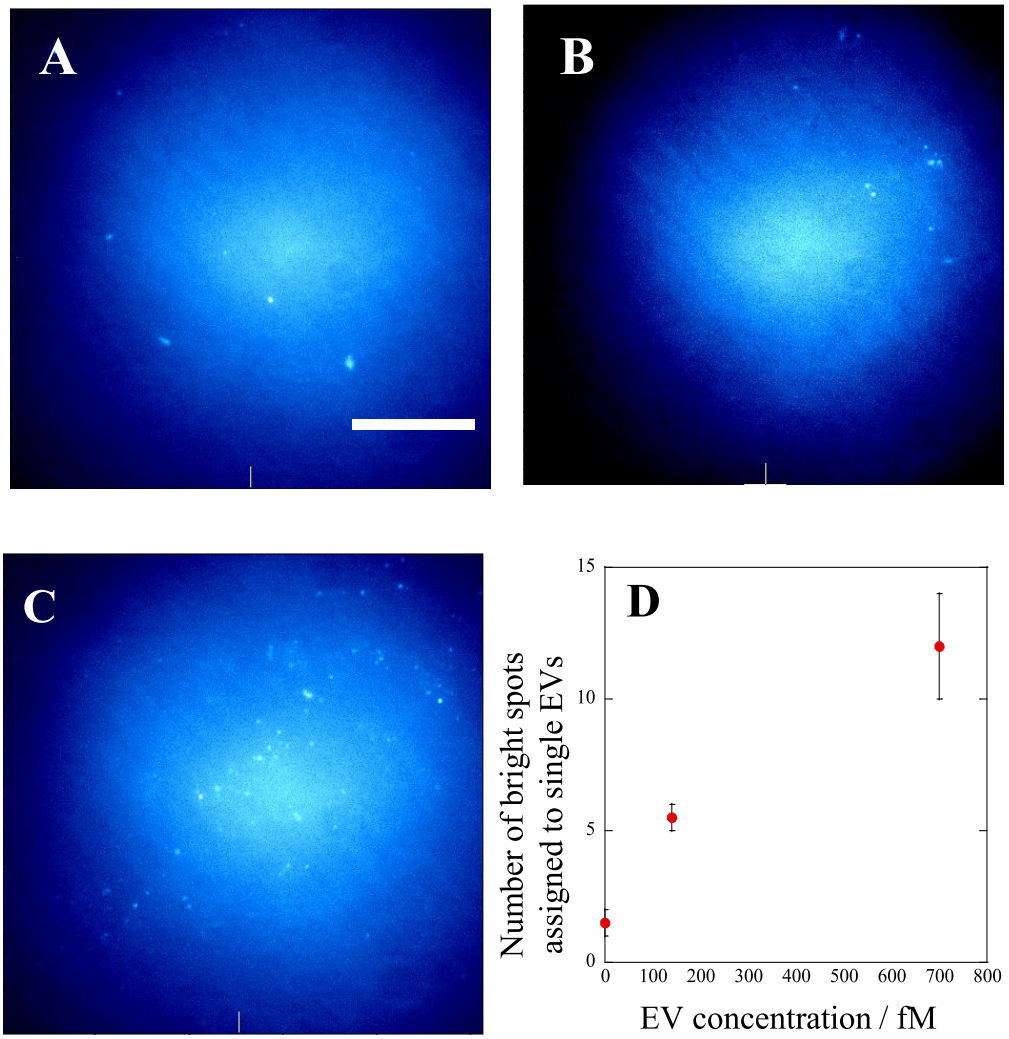

Figure 7. Fluorescence images of single EVs detected with the PE-anti-CD81 antibody on the plasmonic chip using the epifluorescence system from EV solutions of (A) 0, (B) 140, and (C) 700 fM. Bars correspond to 20 μm. After analysis of these images, the number of single EVs was plotted against the EV solution concentrations (D).

adsorption of aggregates of APC-CD9. The capture interface is required to suppress nonspecific adsorption for accurate evaluation of single EVs.

On the other hand, fluorescence images were observed at two more kinds of interfaces, i.e., a protein G interface without capture antibody (Figure S2) and an anti-IL 6 antibody interface bound to the protein G layer (Figure S3). The numbers of bright points with FWHM less than the threshold were individually only one at both interfaces even for EV solutions prepared at 280 fM. The results of few EVs nonspecifically adsorbed to these surfaces showed the highly binding specificity between the CD63 in EVs and the anti-CD 63 antibody (capture interface). The capture interface of the anti-CD63/protein G/PDA/plasmonic chip works well to bind EVs specifically.

Detection of Single EVs by Epifluorescence Imaging with PE-Anti-CD81 on a PDA-Coated Silver Plasmonic Chip. Single EVs were detected with CD81 antibodies. PE-anti-CD81 was used to detect single EVs under an epifluorescence microscope. Fluorescence images observed on three sheets of plasmonic chips for 0, 140, and 700 fM EV solutions are shown in Figure 7A−C. The FWHM values were calculated for the bright spots inside the bull's eye patterns of the fluorescent images. The threshold for distinguishing between aggregates and single EVs was 545 nm in the wavelength range for PE (Table 1). As shown in Figure 7D, a positive correlation was observed between the number of single EVs and the EV concentrations in the injected solution. The number of single EVs was accurately detected by targeting CD81 different membrane proteins from CD9. However, as with the case of APC-Anti-CD9, nonspecific adsorption of PE-CD81 was not completely suppressed. These results led to the development of a new capture interface and the observation technique using fluorescence microscopy.

Single-EV Detection by Epifluorescence Imaging Using Anti-APC-CD9 at the MIP-Based Capture Interface on the Gold Plasmonic Chip. To overcome the nonspecific adsorption not suppressed by the PDA interface, MIP was used for the capture interface (Figure 3).[35] In this interface, capture antibodies were immobilized within the nanocavity prepared by molecular imprinting-based technology using the modified silica nanospheres as the cavity former and biocompatible MPC monomer to form a polymer matrix around the cavity. Each bright spot was analyzed in the fluorescent images of APC-anti-CD9 antibody-labeled EVs, as shown in Figure 8A−C. Bright spots with FWHM values below

https://doi.org/10.1021/acsomega.4c05678
ACS Omega 2024, 9, 44396−44406

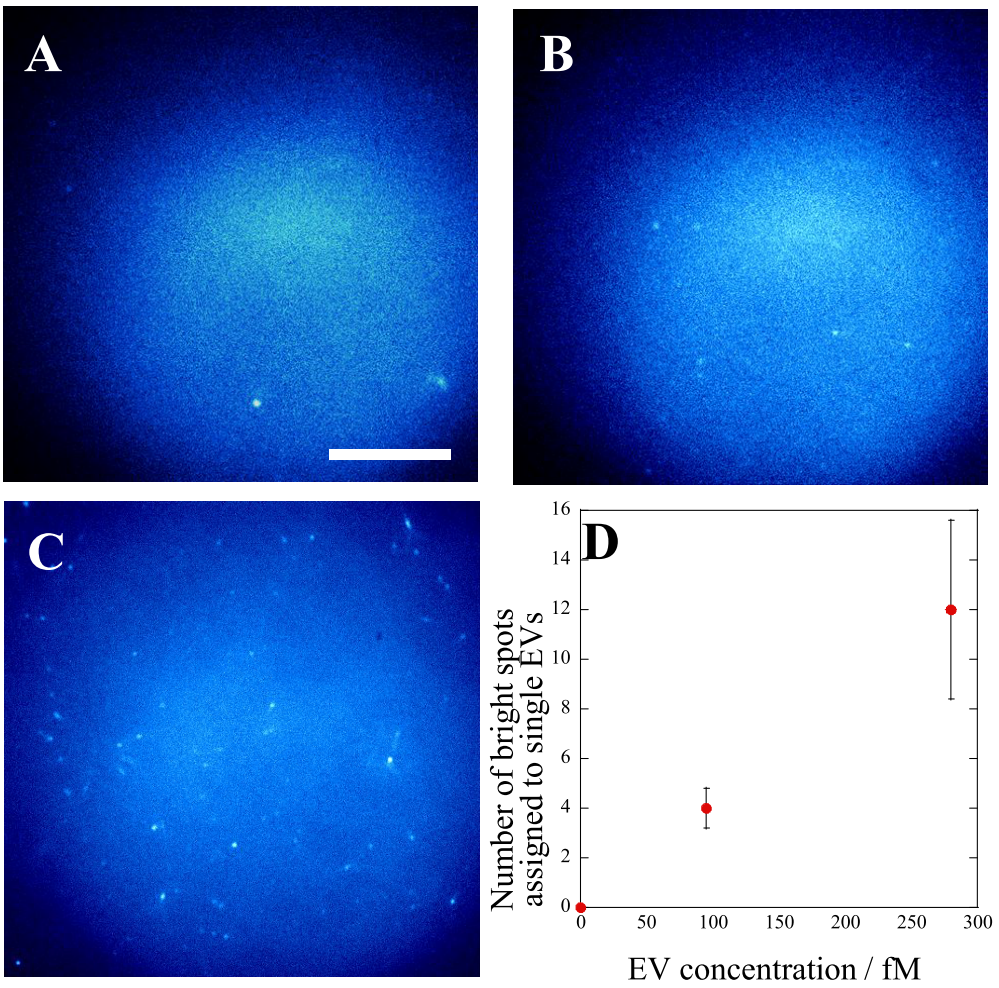

Figure 8. Fluorescence images of single EVs detected with the APC-CD9 antibody on the plasmonic chip with the MIP-based capture interface using the epifluorescence system at EV solutions of (A) 0, (B) 95, and (C) 280 fM. Bars correspond to 20 μm. After analysis of these images, the number of single EVs was plotted against the EV solution concentrations (D).

510 nm were not observed in the fluorescence images for the reference solution (Figure 8D). Therefore, nonspecific adsorption of aggregates of the detection antibody was sufficiently suppressed at the MIP interface, and the specificity was improved compared to the PDA film. These results indicated that the biocompatible MPC polymer-based interface effectively suppresses nonspecific binding.[36] Furthermore, a positive correlation was observed between the concentration of EVs in the solution and the number of EVs captured by the sandwich assay, similar to the relationship detected for the PDA interface. A single EV was sensitively detected at the interface, and nonspecific adsorption was well suppressed. Sensitive single-EV detection on the MIP-based capture interface suggests the synergetic contribution of the specific localization of the captured antibody in the silica-nanosphere-templated imprinted cavity and the suppression of nonspecific binding by the MPC polymer matrix. However, the MIP platform was coated with a thin gold layer, and the off-resonance conditions due to the wavelength dependence of the dielectric constant of gold prevented expansion of the system to excitation wavelengths shorter than 550 nm, which is different from the silver layer. Therefore, as the next strategy, the observation technique was improved for high-sensitivity detection by suppressing nonspecific adsorption.

Single-EV Detection by Transmitted-Light Imaging with APC-Anti-CD9 on a PDA-Coated Silver Plasmonic Chip. Nonspecific adsorption of aggregates of labeled antibodies was included among bright spots assigned to single EVs captured on the PDA-coated chip viewed by epifluorescence imaging. To improve the accuracy of single-EV detection, bright spots were detected with the same sandwich assay and viewed by using fluorescence microscopy under transmitted light. Fluorescence peak intensity and FWHM values were analyzed for each bright spot on the bull's eye patterns of the fluorescent images (Figure 9A–C). Bright spots with FWHM values less than the 523 nm threshold were regarded as APC-anti-CD9 antibody-labeled single EVs. As shown in Figure 9D, the relationship between the number of bright spots assigned as single EVs and the EV concentration of the injected solutions (0 M, 95 fM, and 280 fM) was a positive correlation. The APC-anti-CD9 concentration was the same for each EV solution, but the number of bright spots depended on the EV concentration. Therefore, single EVs were captured and detected on a plasmonic chip using this method. Furthermore, quantitative detection was achieved for a wide range of EV concentrations. The linearity was confirmed to be continued at a concentration as high as 1400 fM, in which the mean values of 26 ± 8 EVs were obtained for four sheets of plasmonic chips (Figure S7). While some bright spots below

https://doi.org/10.1021/acsomega.4c05678
ACS Omega 2024, 9, 44396−44406

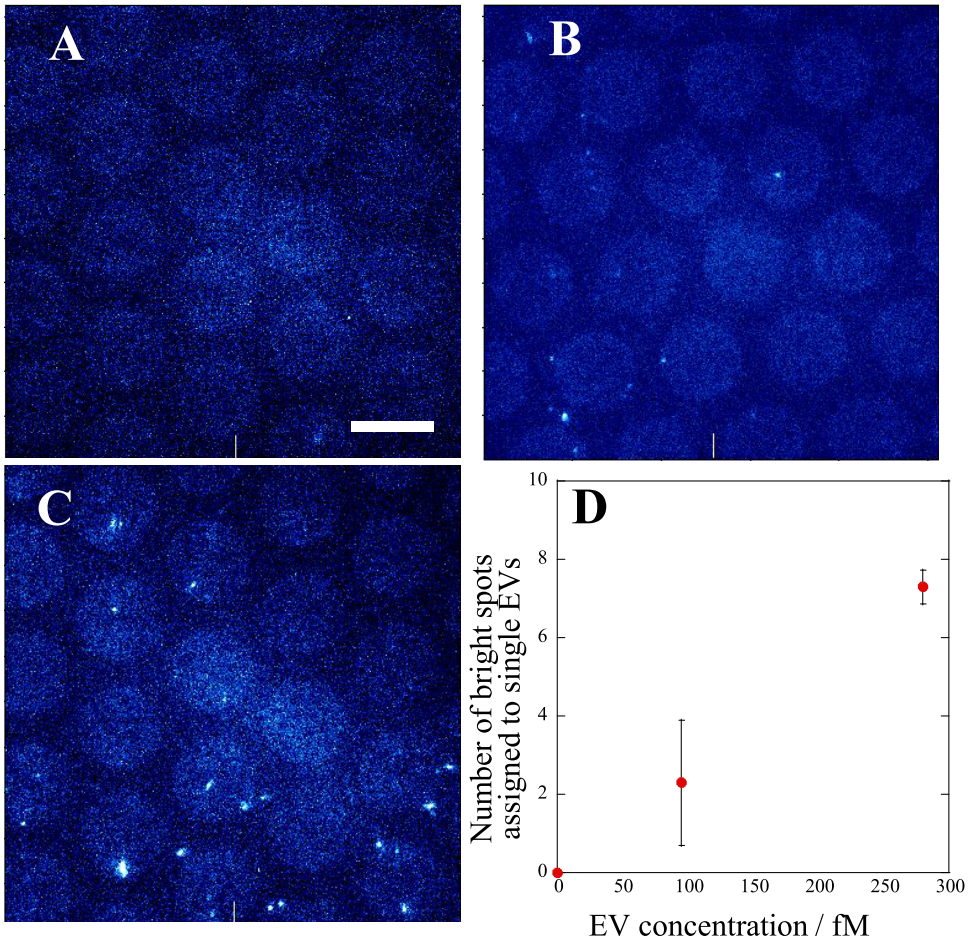

Figure 9. Fluorescence images of single EVs detected with the APC-CD9 antibody on the plasmonic chip using the transmitted-light system at EV solutions of (A) 0, (B) 95, and (C) 280 fM. Bars correspond to 20 μm. After analysis of these images, the number of single EVs was plotted against the EV solution concentrations (D).

the threshold were also derived from aggregates of labeled antibodies and EVs in the epifluorescence system, these nonspecific bright spots were not observed in the transmitted system; i.e., the number of bright spots counted in the reference solution was 0. The reasons are considered as follows: The fluorescence enhancement factor of the bull's eye pattern to the flat area without pattern was 3−5 times[30] and 20 times[31] for epi-mode and transmitted mode under the fluorescence microscopic observation of nanofluorospheres using the Cy5 filter and 100× objective, respectively. The fluorescence intensity of a fluorescently labeled single EV was too small to be detected and precisely analyzed on the flat area in the transmitted mode; therefore, the enhancement factor was not evaluated for single-EV detection. However, this large enhancement effect in the transmitted mode is considered to contribute to suppressing detection of nonspecific adsorption of aggregates compared to that in the epi-mode. Furthermore, aggregates adhering to the upside glass cover except for the plasmonic pattern were not observed as bright spots in the transmitted-light system, and fluorescent images of labeled EVs were mainly obtained by the plasmon-field enhancement. The EV numbers detected by epi-mode and transmitted mode were 16 ± 2.6 and 7.3 ± 0.4 at 280 fM, respectively. Considering the number of bright points assigned to aggregates except for single EVs in the reference solution under the epi-mode of 3 ± 1 EVs, the difference is evaluated to be a few. The above results show the superiority of the fluorescence observation in the transmitted-light system used in this study, and the sandwich assay improved the accuracy of the system.

Single-EV Detection by Transmitted-Light Imaging with PE-Anti-CD81 on a PDA-Coated Silver Plasmonic Chip. To precisely observe single EVs and investigate the positive correlation between the EV concentration and the number of single EVs with both APC-anti-CD9 and other fluorescence-labeled antibodies, we changed the target membrane protein to CD81 and used PE-anti-CD81 as a detection antibody under transmitted-light microscopy. As shown in Figure 10A−C, bright spots with FWHMs less than the 562 nm threshold were assigned as PE-anti-CD81 antibody-labeled single EVs. The number of bright spots at the reference solution was not 0 but well suppressed to less than one. Similar to the results of single-EV detection with APC-anti-CD9, the relationship between the EV concentrations and the numbers of single EVs was positive correlation and highly reproducible, as shown in Figure 10D. Furthermore, considering the number of aggregates in the reference solution under the epi-mode of 1.5 ± 0.5 EVs and the large standard deviation at 280 fM under transmitted mode, the relation curves almost coincide between two kinds of observation modes. On the other hand, the above results also show the superiority of the fluorescence observation in the transmitted-light system as with the APC-CD9 detection.

https://doi.org/10.1021/acsomega.4c05678
ACS Omega 2024, 9, 44396−44406

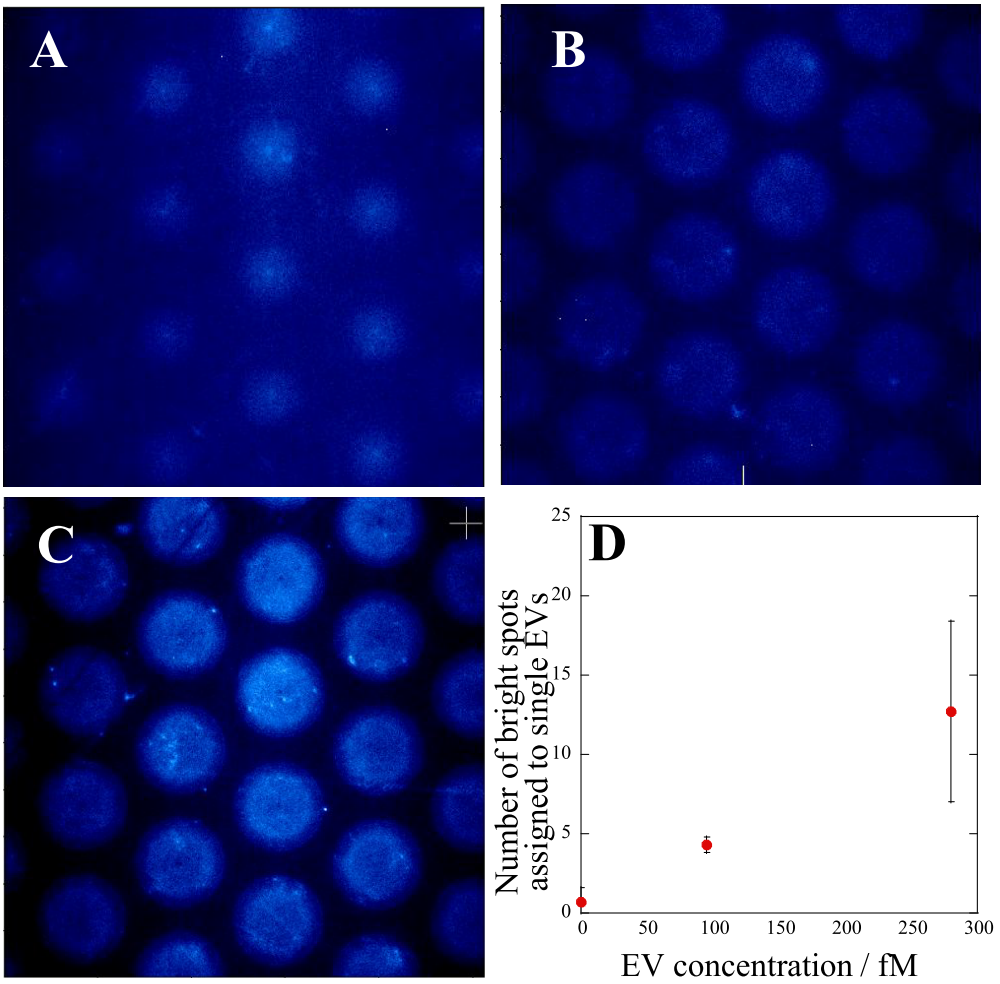

Figure 10. Fluorescence images of single EVs detected with the PE-anti-CD81 antibody on the plasmonic chip using the transmitted-light system at EV solutions of (A) 0, (B) 95, and (C) 280 fM. Bars correspond to 20 μm. After analysis of these images, the number of single EVs was plotted against the EV solution concentrations (D).

Single-EV Detection by Transmitted-Light Imaging with APC-Anti-CD9 and PE-Anti-CD81 on a PDA-Coated Silver Plasmonic Chip. CD9 and CD81 were simultaneously bound with fluorescence-labeled antibodies for a single-EV multicolor assay. Fluorescence images at 560 fM EV solutions mixed with the two detection antibodies were observed under each experimental condition, and bright spots with FWHM values below the respective threshold values were assigned to single EVs. As shown in Figure 11, No. 1−4 bright spots with FWHM values below the threshold were detected at the identical position under both observation conditions (Cy5 and GFP filters). No. 5−8 bright spots were confirmed on only the GFP filter. As shown in bright spots of No. 1−8, EVs bound with both labeled antibodies and with one were mixed. Identical bright spots observed with both fluorescent filters support the validity of the measurement and analysis methods introduced in this study for single-EV detection. Such a multitarget analysis of single EVs is essential for the application of this method to clinical diagnosis.

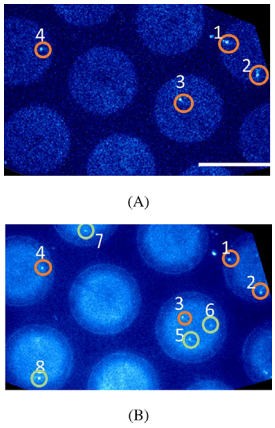

Figure 11. Fluorescence images of single EVs detected with both the APC-anti-CD9 and PE-anti-CD81 antibodies on plasmonic chips using the transmitted-light system and the (A) Cy5 filter or (B) GFP filter. Bar corresponds to 20 μm.

CONCLUSIONS

Although single EVs are difficult to detect with a conventional optical microscope because of their small size, single-EV detection can be useful for the diagnosis and prediction of diseases such as cancer. Therefore, we developed a technique in which fluorescently labeled EVs were captured on a plasmonic chip and observed as bright spots using GC-SPR field-enhanced fluorescence under a fluorescence microscope. The advantages of the detection method studied here are no pretreatment of isolating EVs from free labeled antibodies and

https://doi.org/10.1021/acsomega.4c05678
ACS Omega 2024, 9, 44396−44406

are quantitative, rapid, and simple detection. In the sandwich immunoassay for different target membrane proteins, i.e., CD9 and CD81, FWHMs of bright spots were analyzed, and bright spots smaller than the experimentally determined threshold were assigned to single EVs. A positive correlation was observed for both CD9 and CD81 between the number of single EVs (bright spots) and the EV concentration in epifluorescence and transmitted-light systems, indicating that the method is quantitative. The nonspecific adsorption of aggregates of labeled antibodies observed for 0 fM at epifluorescence mode was improved with transmitted-light fluorescence microscopy. In order to detect EVs accurately, an MIP-based capture interface was also available. Furthermore, this transmitted-light system for single-EV detection was used for simultaneous multitarget detection. This technique may be useful for clinical applications because isolated single EVs can be analyzed in a smaller amount of sample solution than that used in the conventional method.

METHODS

Fabrication of Plasmonic Chips. The mold (quartz substrate, custom-made by NTT-AT, Japan) was composed of approximately 2000 bull's-eye patterns of 20 μm in diameter arranged in a hexagonal lattice at 25 μm intervals (center-to-center). The UV-curable resin was dropped onto a glass substrate treated with silane coupling reagent, and the substrate was covered with the mold. After irradiation with UV light (Ushio, Spot Cure, SP-V) for 90 s, the mold was peeled off. The replicas were then ultrasonically cleaned in ethanol for 3 min and baked at 50 °C under reduced pressure (0.1 MPa). Multiple layers of Ti/Ag/Ti/SiO_2 films were deposited on the replica substrates using RF-sputtering equipment (cryovac, custom-made). The photograph of the plasmonic chip, a bright-field image of bull's eye pattern array, and an AFM image around the center structure are shown in Figure 1. The thicknesses of the Ti, Ag, and SiO_2 layers were less than 1, 40 ± 10, and 20 nm, respectively. The Au films (100 ± 20 nm thick) were stable against chemical reagents used for surface modification and were deposited onto the glass substrate to prepare the MIP-based capture interface instead of the silver film.

AFM Measurement of a Single EV. To investigate the dispersion state of EVs bound to plasmonic chips, a mixture solution of dried EVs (lyophilized EV standards from human serum, Hansa Bio Med HBM-PES-30/2) and detection antibody was injected onto the interface of the chip. After single EVs were observed with a fluorescence microscope, the chip surface was dried and analyzed with AFM.

Samples Used for Threshold Determination to Distinguish a Single EV. Fluorescence images of ϕ 200 nm nanoparticles were observed with epi- and transmitted-light fluorescence microscopes to determine the threshold for distinguishing a single EV less than the optical diffraction limit from aggregates by determining the FWHM of the bright spots (Figure S4). Carboxylate-modified microspheres (ϕ = 200 nm, dark red, Thermo Fisher Scientific; excitation peak wavelength/fluorescence peak wavelength = 660 nm/680 nm) and carboxylate-modified microspheres (ϕ = 200 nm, yellow green, Thermo Fisher Scientific; peak excitation wavelength/peak fluorescence wavelength = 505 nm/515 nm) were used. EV solutions (4.5×10^{12} particles/ml) were prepared in phosphate-buffered saline (PBS). To fix carboxylated fluorescent nanoparticles to the plasmonic chip, the SiO_2 surface of the chip was aminated with 1 vol % (3-aminopropyl)-triethoxysilane solution. The threshold value to judge single EVs under every optical system was individually determined from the mean value of FWHM values for bright spots in the fluorescence image of dark red or yellow green taken under the individual condition (Figure S4).

Samples Used for Single-EV Detection. To construct sandwich assays for single-EV detection, a layer of capture antibody was prepared with a PDA film or by an MIP-based interface. A 12 μg/mL dopamine-HCl (Sigma-Aldrich, USA) solution in Tris buffer (NACALAI TESQUE, Japan) was used for the PDA coating. The solution was dropped onto the chip surface and incubated for 20 min followed by washing with Milli-Q water. The chip surface was subsequently incubated with protein G (recombinant, *Escherichia coli*, Merck Millipore, USA) solution for 15 min as the mediator for the capture antibody. Anti-CD63 antibody (Mouse (MEM-259, GeneTex, USA)) solution was added to capture the EVs through CD63, one of the membrane proteins. After rinsing with PBS solution and adding bovine serum albumin (BIODESIGN, Japan) solution to suppress nonspecific adsorption, a premixed solution of purified EVs from human serum (healthy donors) with wide distribution of size (EXOP-500A-1, System Biosciences, USA) (see Figure S5) and two kinds of fluorescently labeled detection antibodies were added directly onto the chip without a special separation process before injection. The original solution of EVs was 14 pM, and each EV solution was diluted with PBS buffer solution for single-EV detection. The anti-CD9 antibody, which was labeled with APC (mouse-mono(SN4), Funakoshi, Japan; APC-anti-CD9), was diluted 1000 times (3.5 nM) with PBS, and the anti-CD81 antibody, which was labeled with PE (Mouse-Mono (1D6), Funakoshi, Japan; PE-anti-CD81), was diluted 5000 times (125 pM) with a PBS solution. After adding the mixed solution and incubation for 15 min, the chip was rinsed with PBS. The concentrations of EVs in the mixed solutions were 95−1400 fM. For the reference solution, a solution without EVs was prepared at the same concentration of detection antibodies used in the EV solutions. The solution was added to the chip using the same procedure (Figure 2).

As the other capture interface, capture antibodies were bound to the cavities formed using silica nanospheres as the cavity former, similar to MIP-based technology as described below.[25] His-tagged silica nanospheres modified with methacryloyl disulfide groups were prepared and dispersed in dry DMSO. Plasmonic chips (10 × 10 mm) coated with a thin gold film were washed with Milli-Q water and ethanol and dried by spraying N_2 gas. The plasmonic chips were immersed in 1:1-mixed solution of amino-EG_6-undecanthiol hydrochloride aqueous solution and 2-(2-bromoisobuthyryloxy)-undecylthiol EtOH solution prepared at 0.5 mM individually and incubated overnight at 25 °C. Isothiocyanobenzyl-NTA dissolved in dry DMSO was diluted with 10 mM carbonate buffer solution (10 mM) and dropped on the chips. After incubation for 2 h, the chips were washed with DMSO and Milli-Q water, and then 4 mM $NiCl_2$ aqueous solution was dropped to form NTA-Ni complexes and rinsed with Milli-Q water. The modified silica nanospheres were dropped on the chips and incubated for 1 h to immobilize the modified nanospheres via Ni complexation.

The MIP-based capture interface was prepared by surface-initiated atom transfer radical polymerization (ATRP) of 2-methacryloyloxyethyl phosphorylcholine (MPC) from the

https://doi.org/10.1021/acsomega.4c05678
ACS Omega 2024, 9, 44396−44406

modified silica nanosphere-immobilized plasmonic chip. The plasmonic chip was placed in a three-necked flat-bottomed flask with a septum, and 50 mM MPC (1 $\mu\Lambda$) and a mixture of 20 mM 2,2′-bipyridyl and 10 mM CuBr2 (1 mL) and PBS (7 mL) were added. After the flask was degassed and filled with argon gas repeatedly, 5 mM L-ascorbic acid (1 mL) was injected to initiate ATRP. The polymerization was carried out for 3 h at 40 °C with weak oscillation. After ATRP, 1 M EDTA-4Na aqueous solution was dropped onto the substrate and left for 15 min. Substrates were then rinsed with Milli-Q water, and 50 mM tris(2-carboxyethyl)phosphine hydrochloride (TCEP) aqueous solution was added dropwise and incubated for 3 h in the dark to cleave the disulfide bonds. The substrate was then immersed in 50 mM acetic acid buffer (pH 4.0) solution containing 0.5 wt % sodium dodecyl sulfate (SDS) for 1 h with shaking. Finally, the substrate was washed with Milli-Q water to obtain the plasmonic chip coated by the MIP-based capture interface.

To introduce the capture antibody into the MIP-based capture interface via protein G, His-tagged protein G was introduced after the addition of 4 mM $NiCl_2$ solution to form an NTA-Ni complex. The capture antibody, anti-CD63 antibody, was bound to protein G to complete the EV capture interface. The sandwich assay was completed by using a solution of EVs mixed with APC-anti-CD9 in advance in the same process as the PDA capture interface (Figure 2).

Fluorescence Microscopy. Fluorescence images were taken with a fluorescence microscope after rinsing the chip surface capturing labeled EVs and adsorbing free labeled antibodies with PBS solution. Fluorescence images of fluorescent nanoparticles were observed as bright spots to determine the threshold for identifying single EVs less than the diffraction limit using an upright microscope (BX51WI, OLYMPUS) equipped with an electron-multiplying charge-coupled device (EM-CCD) camera (Ixon, KSDU897E-BV-TK, ANDOR), and an upright-inverted fluorescence microscope (custom-made composed of BX51 and IX73, OLYMPUS) with an EM-CCD camera (Ixon, DU-888U-#BY, ANDOR), as shown in Figure 4. The former was used for the epifluorescence system, and the latter for the transmitted-light system. In both systems, Hg lamp and cy5 (Cy5-4040C-000, OLYMPUS, excitation wavelength 608−648 nm, emission wavelength 672−712 nm) and GFP (U-MGFPHQ, OLYMPUS, excitation wavelength 460−480 nm, emission wavelength 495−540 nm) filter units were used for excitation light during EV detection with APC and PE, respectively. The 100× (PlanFLN100x, OLYMPUS, numerical aperture (NA) = 0.95) objective was used for fluorescence detection in both systems. For the transmitted fluorescence measurements using the upright-inverted microscope, a 40× (LUCPlanFL40x, NA = 0.60) objective lens was used for illumination. Both optical systems satisfied the surface plasmon resonance condition for the 480 nm-pitch plasmonic chip, and enhanced fluorescence could be detected (Figure S6).

■ ASSOCIATED CONTENT

Supporting Information

The Supporting Information is available free of charge at https://pubs.acs.org/doi/10.1021/acsomega.4c05678.

Additional experimental details and analysis method, including experimental and theoretical results shown by fluorescence images and graphs (PDF)

■ AUTHOR INFORMATION

Corresponding Author

Keiko Tawa − *Graduate School of Science and Technology, Kwansei Gakuin University, Sanda, Hyogo 669-1330, Japan*; orcid.org/0000-0002-5736-1187; Email: ktawa@kwansei.ac.jp

Authors

Kazuma Fukutomi − *Graduate School of Science and Technology, Kwansei Gakuin University, Sanda, Hyogo 669-1330, Japan*

Eri Fujimoto − *Graduate School of Science and Technology, Kwansei Gakuin University, Sanda, Hyogo 669-1330, Japan*

Masaya Shimokawatoko − *Graduate School of Science and Technology, Kwansei Gakuin University, Sanda, Hyogo 669-1330, Japan*

Eri Takano − *Graduate School of Engineering, Kobe University, Kobe 657-8501, Japan*

Hirobumi Sunayama − *Graduate School of Engineering, Kobe University, Kobe 657-8501, Japan*; orcid.org/0000-0001-5145-2312

Toshifumi Takeuchi − *Innovation Commercialization Division, Kobe University, Kobe 657-8501, Japan*; orcid.org/0000-0002-5641-2333

Complete contact information is available at: https://pubs.acs.org/10.1021/acsomega.4c05678

Author Contributions

The manuscript was written through the contributions of all authors listed in the following. All authors have approved the final version of the manuscript. K. Fukutomi contributed to formal analysis, investigation, visualization, and writing of the original draft. E. Fujimoto contributed to formal analysis, investigation, visualization, and methodology. M. Shimokawadoko contributed to formal analysis, investigation, and visualization. E. Takano and H. Sunayama contributed to materials, conceptualization, and writing review and editing. T. Takeuchi contributed to conceptualization, funding acquisition, project administration, and writing review and editing. K. Tawa contributed to conceptualization, funding acquisition, methodology, project administration, supervision, and writing review and editing.

Funding

This study was funded by JSPS KAKENHI Grant Numbers 16H02092and 19H00854.

Notes

The authors declare no competing financial interest.

■ ACKNOWLEDGMENTS

K.F., E.F., M.S., and K.T. thank Toyo Gosei for providing the UV-curable resin.

■ REFERENCES

(1) Valadi, H.; Ekström, K.; Bossios, A.; Sjöstrand, M.; Lee, J. J.; Lötvall, J. O. EV-Mediated Transfer of Mrnas and MicroRNAs is a Novel Mechanism of Genetic Exchange Between Cells. *Nat. Cell Biol.* **2007**, *9*, 654−659.

(2) Vlassov, A. V.; Magdaleno, S.; Setterquist, R.; Conrad, R. EVs: Current Knowledge of their Composition, Biological Functions, and Diagnostic and Therapeutic Potentials. *Biochim. Biophys. Acta* **2012**, *1820*, 940−948.

(3) Kowal, J.; Tkach, M.; Théry, C. Biogenesis and Secretion of EVEVs. *Curr. Opin Cell Biol.* **2014**, *29*, 116−125.

(4) Denzer, K.; Kleijmeer, M. J.; Heijnen, H. F. G.; Stoorvogel, W.; Geuze, H. J. EV: From Internal Vesicle of the Multivesicular Body to Intercellular Signaling Device. *J. Cell Sci.* **2000**, *113*, 3365−3374.
(5) Kalluri, R.; LeBleu, V. S. The Biology, Function, and Biomedical Applications of EVs. *Science* **2020**, *367*, 640.
(6) Tkach, M.; Théry, C. Communication by Extracellular Vesicles: Where We are and Where We Need to Go. *Cell* **2016**, *164* (6), 1226−1232.
(7) Hessvik, N. P.; Llorente, A. Current Knowledge on EVEV Biogenesis and Release. *Cell. Mol. Life Sci.* **2018**, *75*, 193−208.
(8) Pegtel, D. M.; Gould, S. J. Exosomes. *Annu. Rev. Biochem.* **2019**, *88*, 487−514.
(9) György, B.; Szabó, T. G.; Pásztói, M.; Pál, Z.; Misják, P.; Aradi, B.; László, V.; Pállinger, E.; Pap, E.; Kittel, A.; Nagy, G.; Falus, A.; Buzás, E. I. Membrane Vesicles, Current State-of-the-EVArt: Emerging Role of Extracellular Vesicles. *Cell. Mol. Life Sci.* **2011**, *68*, 2667−2688.
(10) Hoshino, A.; Kim, H. S.; Bojmar, L.; Gyan, K. E.; Cioffi, M.; Hernandez, J.; Zambirinis, C. P.; Rodrigues, G.; Molina, H.; Heissel, S.; Mark, M. T.; Steiner, L.; Benito-Martin, A.; Lucotti, S.; Di Giannatale, A.; Offer, K.; Nakajima, M.; Williams, C.; Nogués, L.; Vatter, F. A. P.; Hashimoto, A.; Davies, A. E.; Freitas, D.; Kenific, C. M.; Ararso, Y.; Buehring, W.; et al. Extracellular Vesicle and Particle Biomarkers Define Multiple Human Cancers. *Cell* **2020**, *182* (4), 1044−1061.e18.
(11) Boukouris, S.; Mathivanan, S. EVs in Bodily Fluids are a Highly Stable Resource of Disease Biomarkers. *Proteomics Clin Appl.* **2015**, *9*, 358−367.
(12) Bobrie, A.; Colombo, M.; Raposo, G.; Théry, C. EV Secretion: Molecular Mechanisms and Roles in Immune Responses. *Traffic* **2011**, *12*, 1659−1668.
(13) Barile, L.; Vassalli, G. EVs: Therapy Delivery Tools and Biomarkers of Diseases. *Pharmacol Ther* **2017**, *174*, 63−78.
(14) Shao, H. L.; Im, H.; Castro, C. M.; Breakefield, X.; Weissleder, R.; Lee, H. H. New Technologies for Analysis of Extracellular Vesicles. *Chem. Rev.* **2018**, *118*, 1917−1950.
(15) Caby, M. P.; Lankar, D.; Vincendeau-Scherrer, C.; Raposo, G.; Bonnerot, C. Exosomal-Like Vesicles are Present in Human Blood Plasma. *Int. Immunol.* **2005**, *17*, 879−887.
(16) Colombo, M.; Raposo, G.; Théry, C. Biogenesis, Secretion, and Intercellular Interactions of EVs and Other Extracellular Vesicles. *Annu. Rev. Cell Dev. Biol.* **2014**, *30*, 255−289.
(17) Escrevente, C.; Keller, S.; Altevogt, P.; Costa, J. Interaction and Uptake of EVs by Ovarian Cancer Cells. *BMC Cancer* **2011**, *11*, 108.
(18) Shurtleff, M. J.; Temoche-Diaz, M. M.; Karfilis, K. V.; Ri, S.; Schekman, R. Y-Box Protein 1 Is Required to Sort microRNAs into EVs in Cells and in a Cell-Free Reaction. *eLife* **2016**, *5*, 5.
(19) Lane, R. E.; Korbie, D.; Anderson, W.; Vaidyanathan, R.; Trau, M. Analysis of EVEV Purification Methods Using a Model Liposome System and Tunable-Resistive Pulse Sensing. Scientific report. *Sci. Rep* **2015**, *5*, 7639.
(20) Burnette, W. N. 'Western Blotting': Electrophoretic Transfer of Proteins from Sodium Dodecyl Sulfate-Polyacrylamide Gels to Unmodified Nitrocellulose and Radiographic Detection with Antibody and Radioiodinated Protein A. *Anal. Biochem.* **1981**, *112*, 195−203.
(21) Adams, A. N.; Clark, M. F. Characteristics of the Microplate Method of Enzyme-Linked-Immunosorbent-Assay for the Detection of Plant-Viruses. *J. Gen. Virol.* **1977**, *34*, 475−483.
(22) Liu, X.; Zong, Z.; Xing, M.; Liu, X.; Li, J.; Liu, D. pH-Mediated Clustering of EVs: Breaking Through the Size Limit of EV Analysis in Conventional Flow Cytometry. *Nano Lett.* **2021**, *21*, 8817−8823.
(23) Im, H.; Shao, H. L.; Park, Y. I.; Peterson, V. M.; Castro, C. M.; Weissleder, R.; Lee, H. Label-Free Detection and Molecular Profiling of EVEVs with a Nano-Plasmonic Sensor. *Nat. Biotechnol.* **2014**, *32* (U219), 490.
(24) Zhu, L.; Wang, K.; Cui, J.; Liu, H.; Bu, X. L.; Ma, H. L.; Wang, W. Z.; Gong, H.; Lausted, C.; Hood, L.; Yang, G.; Hu, Z. Label-Free Quantitative Detection of Tumor-Derived EVs through Surface Plasmon Resonance Imaging. *Anal. Chem.* **2014**, *86*, 8857−8864.
(25) Liang, H.; Wang, X.; Li, F.; Xie, Y.; Shen, J.; Wang, Z.; Huang, Y.; Lin, S.; Chen, J.; Zhang, L.; Jiang, B.; Xing, J.; Zhu, J. Label-free plasmonic metasensing of PSA and exosomes in serum for rapid high-sensitivity diagnosis of early prostate cancer. *Biosens. Bioelectron.* **2023**, *235*, No. 115380.
(26) Min, J.; Son, T.; Hong, J.-S.; Cheah, P. S.; Wegemann, A.; Murlidharan, K.; Weissleder, R.; Lee, H.; Im, H. Plasmon-Enhanced Biosensing for Multiplexed Profiling of Extracellular Vesicles. *Adv. Biosys.* **2020**, *4*, No. 2000003.
(27) Amrhein, K.; Taylor, M. L.; Wilson, R.; Gallops, C. E.; Annamer, A.; Vinduska, V.; Kwizera, E. A.; Zhang, H.; Wang, H.; Hoang, T. B.; Huang, X. Dual Imaging Single Vesicle Surface Protein Profiling and Early Cancer Detection. *ACS Appl. Mater. Interfaces* **2023**, *15*, 2679−2692.
(28) Tawa, K.; Yamamura, S.; Sasakawa, C.; Shibata, I.; Kataoka, M. Sensitive Detection of Cell Surface Membrane Proteins in Living Breast Cancer Cells Using Multicolor Fluorescence Microscopy with a Plasmonic Chip. *ACS Appl. Mater. Interfaces* **2016**, *8*, 29893−29898.
(29) Tawa, K.; Yasui, C.; Hosokawa, C.; Aota, H.; Nishii, J. In Situ Sensitive Fluorescence Imaging of Neurons Cultured on a Plasmonic Dish Using Fluorescence Microscopy. *ACS Appl. Mater. Interfaces* **2014**, *6*, 20010−20015.
(30) Tawa, K.; Izumi, S.; Sasakawa, C.; Hosokawa, C.; Toma, M. Enhanced Fluorescence Microscopy with the Bull's Eye-Plasmonic Chip. *Opt Express* **2017**, *25*, 10622−10631.
(31) Nagasue, T.; Shinohara, T.; Hasegawa, S.; Imura, K.; Tawa, K. Nanoantenna Effect Dependent on the Center Structure of Bull's Eye-type Plasmonic Chip. *Opt. Express* **2022**, *30*, 7526−7538.
(32) Raether, H. *Surface Plasmons on Smooth and Rough Surfaces and on Gratings*; Springer-Verlag: Heidelberg, Germany, 1988.
(33) Knoll, W. Interfaces and Thin Films as Seen by Bound Electromagnetic Waves. *Annu. Rev. Phys. Chem.* **1998**, *49*, 569−638.
(34) Tawa, K.; Kondo, F.; Sasakawa, C.; Nagae, K.; Nakamura, Y.; Nozaki, A.; Kaya, T. Sensitive Detection of a Tumor Marker, α-Fetoprotein, with a Sandwich Assay on a Plasmonic Chip. *Anal. Chem.* **2015**, *87*, 3871−3876.
(35) Takeuchi, T.; Mori, K.; Sunayama, H.; Takno, E.; Kitayama, Y.; Shimizu, T.; Hirose, Y.; Inubushi, S.; Sasaki, R.; Tanino, H. Antibody-Conjugated Signaling Nanocavities Fabricated by Dynamic Molding for Detecting Cancers Using Small Extracellular Vesicle Markers from Tears. *J. Am. Chem. Soc.* **2020**, *142*, 6617−6624.
(36) Ishihara, K. Revolutionary advances in 2-methacryloyloxyethyl phosphorylcholine polymers as biomaterials. *J. Biomed. Mater. Res. Part A* **2019**, *107A*, 933−943.

https://doi.org/10.1021/acsomega.4c05678
ACS Omega 2024, 9, 44396−44406